Mitochondrial calcium uniporter in *Drosophila* transfers calcium between the endoplasmic reticulum and mitochondria in oxidative stress-induced cell death

Received for publication, October 31, 2016, and in revised form, July 13, 2017 Published, Papers in Press, July 18, 2017, DOI 10.1074/jbc.M116.765578

Sekyu Choi[‡1], **Xianglan Quan**[§1,2], **Sunhoe Bang**[‡1,3], **Heesuk Yoo**[‡3], **Jiyoung Kim**[‡], **Jiwon Park**[‡3], **Kyu-Sang Park**[§4], **and Jongkyeong Chung**[‡3,5]

From the [‡]*National Creative Research Initiatives Center for Energy Homeostasis Regulation, Institute of Molecular Biology and Genetics and School of Biological Sciences, Seoul National University, Seoul 08826, Korea and the* [§]*Department of Physiology, Yonsei University Wonju College of Medicine, Wonju, Gangwon-Do 26426, Korea*

Edited by John M. Denu

Mitochondrial calcium plays critical roles in diverse cellular processes ranging from energy metabolism to cell death. Previous studies have demonstrated that mitochondrial calcium uptake is mainly mediated by the mitochondrial calcium uniporter (MCU) complex. However, the roles of the MCU complex in calcium transport, signaling, and dysregulation by oxidative stress still remain unclear. Here, we confirmed that *Drosophila* MCU contains evolutionarily conserved structures and requires essential MCU regulator (EMRE) for its calcium channel activities. We generated *Drosophila* MCU loss-of-function mutants, which lacked mitochondrial calcium uptake in response to caffeine stimulation. Basal metabolic activities were not significantly affected in these MCU mutants, as observed in examinations of body weight, food intake, body sugar level, and starvation-induced autophagy. However, oxidative stress-induced increases in mitochondrial calcium, mitochondrial membrane potential depolarization, and cell death were prevented in these mutants. We also found that inositol 1,4,5-trisphosphate receptor genetically interacts with *Drosophila* MCU and effectively modulates mitochondrial calcium uptake upon oxidative stress. Taken together, these results support the idea that *Drosophila* MCU is responsible for endoplasmic reticulum-to-mitochondrial calcium transfer and for cell death due to mitochondrial dysfunction under oxidative stress.

Mitochondrial Ca^{2+} is a key regulator for cellular metabolic functions by activating Krebs cycle dehydrogenases, metabolite shuttle systems, and ATP synthase. However, inappropriately high Ca^{2+} levels in the mitochondrial matrix threaten cell survival by increasing reactive oxygen species (ROS)[6] production and triggering mitochondrial permeability transition (mPT). The main route for Ca^{2+} uptake into mitochondria is through mitochondrial calcium uniporter (MCU), a Ca^{2+}-selective ion channel located at the inner mitochondrial membrane (1), which was originally identified as CCDC109A (2, 3). Recent studies have demonstrated that MCU has a homopentameric structure in which the second transmembrane domain forms a hydrophilic pore across the membrane (4) and the N terminus domain modulates MCU activity by protein–protein interaction and binding divalent cations (5, 6). To counteract the Ca^{2+} influx via MCU, mitochondrial sodium–calcium exchanger (NCLX) provides mitochondrial Ca^{2+} efflux routes by exchanging Ca^{2+} for Na^{+} ions (7). Leucine zipper EF-hand-containing transmembrane protein 1 (LETM1) may also be involved in mitochondrial Ca^{2+} influx or efflux, which is still in a controversy (8–11).

Previous studies have identified multiple regulators of MCU activity, including mitochondrial calcium uptake 1 and 2 (MICU1/2), mitochondrial calcium uniporter regulator 1 (MCUR1), and essential MCU regulator (EMRE). EMRE is a 10-kilodalton mitochondrial inner membrane protein with a single transmembrane domain, which is an essential component that bridges MICU1/2 with MCU (12). The transmembrane helix of EMRE interacts with MCU, and the C terminus of EMRE binds to MICU1 (13). In addition, silencing of EMRE completely abolishes the channel activity of MCU (14). MICU1/2 are Ca^{2+}-binding EF-hand-containing proteins residing in the mitochondrial intermembrane space. They can modulate MCU activity, depending on cytoplasmic Ca^{2+} con-

The authors declare that they have no conflicts of interest with the contents of this article.

This article contains supplemental Figs. S1–S5.

[1] These authors contributed equally to this work and should be considered co-first authors.

[2] Present address: Dept. of Oncology, Affiliated Hospital of Yanbian University, Yanji, Jilin Province 133000, China.

[3] Supported by the BK21 Plus Program from the Ministry of Education (MOE), Korea.

[4] Supported by National Research Foundation of Korea (NRF) Grant 2016R1A2B4014565. To whom correspondence may be addressed: Dept. of Physiology, Yonsei University Wonju College of Medicine, 20 Ilsan-Ro, Wonju, Gangwon-Do 26426, Korea. Tel.: 82-33-741-0294; Fax: 82-33-745-6461; E-mail: qsang@yonsei.ac.kr.

[5] Supported by the National Creative Research Initiatives grant through the National Research Foundation of Korea (NRF) funded by the Ministry of Science, ICT, and Future Planning (MSIP), Korea (Grant 2010-0018291). To whom correspondence may be addressed: Institute of Molecular Biology and Genetics, Seoul National University, 1 Gwanak-Ro, Gwanak-Gu, Seoul 08826, Korea. Tel.: 82-2-880-4399. Fax: 82-2-876-4401; E-mail: jkc@snu.ac.kr.

[6] The abbreviations used are: ROS, reactive oxygen species; MCU, mitochondrial calcium uniporter; IP_3R, inositol 1,4,5-trisphosphate receptor; mPT, mitochondrial permeability transition; MAM, mitochondria-associated ER membrane; $[Ca^{2+}]_{mito}$, mitochondrial matrix Ca^{2+} concentration; MTRP, mitochondria-targeted ratio-pericam; *t*-BuOOH, *tert*-butyl hydroperoxide; Ψ_{mito}, mitochondrial membrane potential; *MCU*^{52}, a null mutant of *MCU*; RPmit4.1, mitochondria-targeted ratio-pericam plasmid; ER, endoplasmic reticulum; DHE, dihydroethidium; RyR, ryanodine receptor; PFA, paraformaldehyde; Ex, excitation; Em, emission.

centration ($[Ca^{2+}]_i$) (15–17). MCUR1 is an inner mitochondrial membrane integral protein binding to MCU and regulates MCU-dependent mitochondrial Ca^{2+} uptake (18) and Ca^{2+} threshold for mPT (19).

Over the last few years, studies on the MCU complex have proposed diverse roles of MCU at the cellular and organism levels, using its genetic ablation and/or pharmacologic inhibition models. Although a loss-of-function mutation of *MCU* in mice exhibited negligible influence on metabolism and cell death (20), further studies revealed that MCU plays an essential role in heart rate acceleration during fight-or-flight response (21), ROS-mediated wound repair (22), and skeletal muscle trophism (23). In pancreatic β-cells, MCU silencing decreases mitochondrial ATP synthesis and impairs the metabolism-secretion coupling (11, 24). In neuronal cells, suppression of MCU relieves ischemia and reperfusion injuries as well as Ca^{2+} excitotoxicity (25, 26). In cardiac cells, however, a loss-of-function mutation of *MCU* did not protect from ischemic injury due to $[Ca^{2+}]_i$ overload despite preserved mitochondrial membrane potential ($\Delta\Psi_m$) and reduced ROS formation (27).

The main source of mitochondrial Ca^{2+} is the endoplasmic reticulum (ER), which has a higher Ca^{2+} level (>400 μM) required for protein folding and Ca^{2+} signaling. Ca^{2+} release from the ER is taken up by mitochondria not only to avoid $[Ca^{2+}]^i$ accumulation but also to stimulate mitochondrial energy metabolism (28). This ER–mitochondrial interaction is mediated by physical contacts between the two organelles via mitochondria-associated ER membrane (MAM) (29, 30). MAM is composed of several proteins, including inositol 1,4,5-trisphosphate receptor (IP_3R), glucose-regulated protein 75 (grp75), porin, and MCU (31). The MAM formation can be expanded in pathologic conditions, such as obesity and diabetes, in which increased ER–mitochondrial Ca^{2+} connection exacerbates ER Ca^{2+} depletion and mitochondrial Ca^{2+} overload (32).

Oxidative stress disrupts cellular Ca^{2+} homeostasis and consequently induces cytotoxicity. Oxidative stress activates IP_3R, stimulates ER Ca^{2+} release, intensifies ER stress, and leads to apoptosis (33, 34). More importantly, oxidative stress plays significant roles in the pathogenesis of various chronic diseases, including neurodegeneration (35). However, the pathophysiological role of Ca^{2+} dysregulation by oxidative stress still remains elusive.

In this study, we generated *Drosophila MCU* loss-of-function mutants for the first time and characterized their phenotypes on metabolism, Ca^{2+} handling, and cell death. We demonstrated that attenuated Ca^{2+} transport from the ER to mitochondria in *MCU* mutants prevents ROS-induced mitochondrial dysfunction and cell death. Because the *Drosophila* system provides powerful tools for genetic studies, our loss-of-function mutants and transgenic flies for MCU and other components of MCU complex would provide crucial information for understanding the regulatory mechanism of mitochondrial Ca^{2+} homeostasis.

Results

Drosophila MCU null mutant is viable

According to a recent report, CG18769 is homologous to mammalian MCU (36). Human and mouse MCU protein sequences are similar to the protein sequence encoded by CG18769 (supplemental Fig. S1*A*). CG18769-encoded protein localizes to mitochondria, and silencing CG18769 decreases mitochondrial Ca^{2+} entry (36, 37). To assess the *in vivo* role of MCU, *Drosophila MCU* loss-of-function mutants were generated by P-element imprecise excision in the 5′-untranslated region of CG18769 using the P(GSV6)GS11565 fly line (Fig. 1*A*). From the 200 excision alleles obtained, we found MCU^{52} mutant, which lacked 1,476 bp (3R14578001–14580477) that encoded the transcription start site and the first exon of *MCU* (Fig. 1, *A* and *B*). In the mutant, MCU mRNA and protein were not detected by quantitative RT-PCR (Fig. 1*C*) and immunoblotting (Fig. 1*D*). Wild-type MCU protein was expressed weakly in embryo stage but strongly in larva, pupa, and adult stages (Fig. 1*E*). MCU^{52} mutant flies were viable and showed a similar survival rate compared with wild-type ones (Fig. 1*E*).

MCU^{52} mutant does not show significant metabolic phenotypes

To find the exclusive role of MCU in *Drosophila* physiology, we investigated metabolic phenotypes of MCU^{52} mutant. First, the body weight of MCU^{52} mutants was not different from that of wild-type flies in both sexes (Fig. 1*F*). The amount of food intake of MCU^{52} mutant was also similar to that of the wild-type fly (Fig. 1*G*). The concentration of circulating sugars in the hemolymph of MCU^{52} mutants was not significantly different from that in wild-type flies (Fig. 1*H*). We also did not observe any detectable changes in starvation-induced autophagy (Fig. 1*I*). Collectively, these results showed that loss of MCU does not alter basal metabolism in *Drosophila*.

The Ca^{2+} channel activity of MCU is conserved in Drosophila

To assess mitochondrial Ca^{2+} uptake in a physiological context, we measured mitochondrial matrix Ca^{2+} concentration ($[Ca^{2+}]_{mito}$) in a larval muscle expressing mitochondria-targeted ratio-pericam (MTRP), a genetically encoded Ca^{2+} indicator targeted to the mitochondrial matrix (38). MTRP was specifically expressed in muscle tissues by *Mef-Gal4* and *UAS-MTRP* (Fig. 2*A*). The localization of expressed MTRP to mitochondria was confirmed with two mitochondria markers, streptavidin (Fig. 2*B*) and ATP5a (supplemental Fig. S2*A*).

To confirm that *Drosophila* MCU is a functional mitochondrial Ca^{2+} uptake route, we compared $[Ca^{2+}]_{mito}$ increase in muscle tissues of control, MCU^{52} mutant, and MCU^{52} mutant expressing exogenous *Drosophila* wild-type *MCU* (Fig. 2*C*). Caffeine was used to stimulate Ca^{2+} release from the ER, inducing elevation of cytosolic (supplemental Fig. S3*A*) and mitochondrial Ca^{2+} levels (Fig. 2*D*). In control larvae, $[Ca^{2+}]_{mito}$ was increased sharply after caffeine stimulation and slowly returned to the basal level (Fig. 2*D*). However, although caffeine-induced $[Ca^{2+}]_i$ changes were not significantly different between control and MCU^{52} mutant larvae (supplemental Fig. S3A), MCU^{52} mutant failed to elicit any $[Ca^{2+}]_{mito}$ change upon caffeine stimulation (Fig. 2, *D* and *E*). Furthermore, when exogenous *Drosophila MCU* was overexpressed in MCU^{52} mutant, the absence of caffeine-induced $[Ca^{2+}]_{mito}$ response in the mutant was completely rescued (Fig. 2, *D* and *E*). These results consistently demonstrate the indispensable role of *Drosophila* MCU in mitochondrial Ca^{2+} uptake.

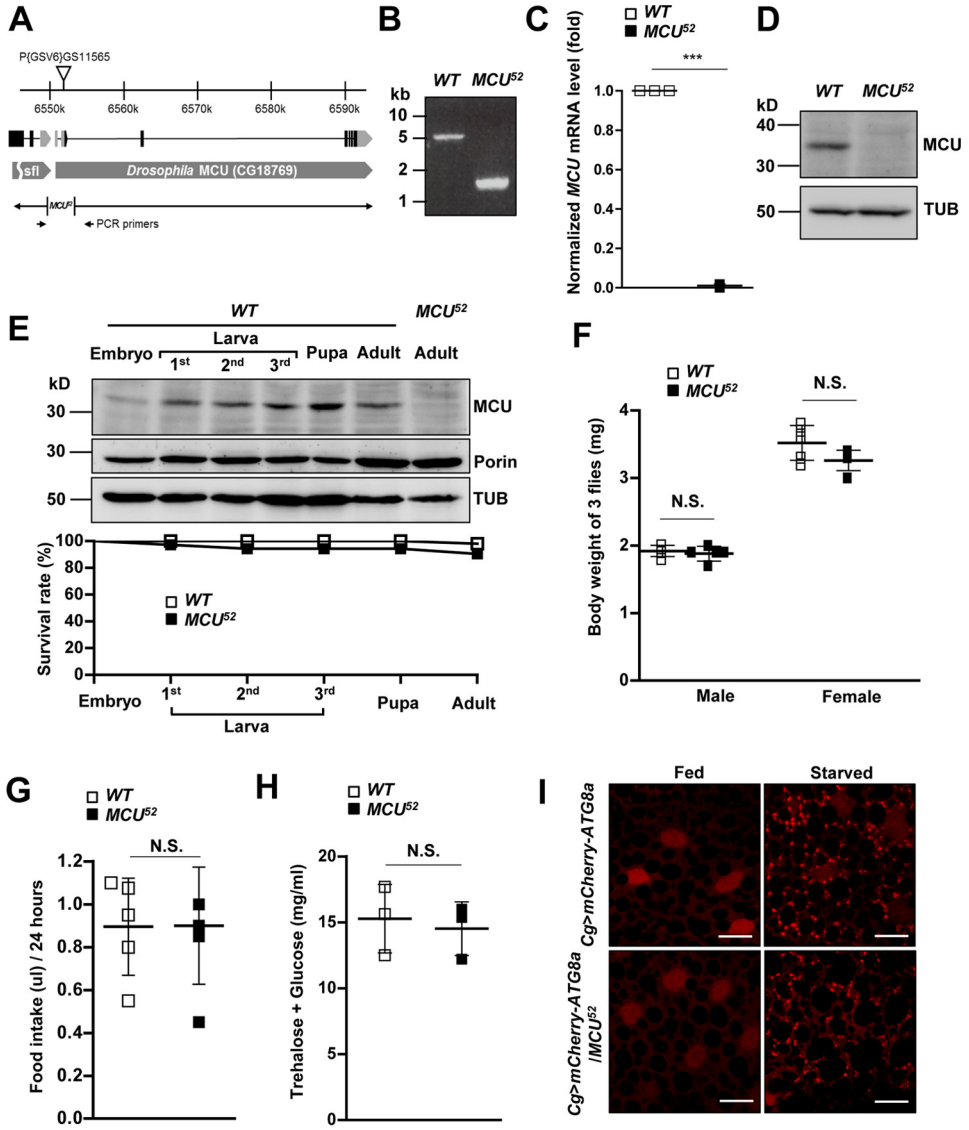

Figure 1. MCU mutant shows normal metabolism. *A*, schematic representation of *Drosophila* MCU genomic locus and the genomic deletion region of MCU^{52}. Exons are indicated by *boxes*, and the coding regions are *colored black*. *B*, PCR result to detect genomic DNA deletion around the transcription start site of *MCU* using the primer set in *A*. *C*, quantitative RT-PCR analysis of *MCU* transcript in wild-type control and MCU^{52} flies ($n = 3$). *D*, immunoblotting by anti-MCU and anti-β-tubulin (*TUB*) antibodies in wild-type control and MCU^{52} flies. Tubulin was used as a loading control. *E*, MCU expression and survival rate in various developmental stages. Homogenized samples at the indicated developmental stage were immunoblotted by anti-MCU, anti-porin, and anti-β-tubulin antibodies. Tubulin and porin were used as loading controls. The survival rate of wild-type control and MCU^{52} mutant during development is shown in the *bottom panel*. *F*, body weights of wild-type control and MCU^{52} ($n = 5$). *G*, food intake for 24 h by wild-type control and MCU^{52} flies ($n = 5$–6). *H*, hemolymph concentration of trehalose and glucose in wild-type control and MCU^{52} flies ($n = 3$). *I*, mCherry-ATG8a signal images illustrating starvation-induced autophagy in larval fat body of MCU null flies (*Cg>mCherry-ATG8a;* MCU^{52}/MCU^{52}) and control flies (*Cg>mCherry-ATG8a*) in fed and starved conditions. The starvation-induced autophagy assays were conducted using more than 10 flies. *Scale bars*, 20 μm. ***, $p < 0.001$. *N.S.*, not significant. *Error bars*, S.D.

To test whether *Drosophila* MCU is functionally equivalent to the mammalian MCU, we expressed human *MCU* in the muscle of MCU^{52} mutants (Fig. 2*F*). Similar to the results with *Drosophila MCU*, overexpression of human *MCU* in MCU^{52} mutant larvae resulted in full recovery of $[Ca^{2+}]_{mito}$ response upon caffeine stimulation (Fig. 2, *G* and *H*). These results demonstrate that *Drosophila* MCU (encoded by CG18769) is a genuine orthologue of human MCU.

MCU has a mitochondrial targeting sequence at its N terminus, two coiled-coil domains, two transmembrane domains, and the DIME motif. Previous studies showed that substitution of two acidic amino acids within the DIME motif resulted in a dominant-negative effect on the uniporter activity of mammalian MCU (39, 40). To test whether the DIME motif in *Drosophila* MCU is also critical for its Ca^{2+} channel activity, we generated a mutant of MCU in the DIME motif (MCU^{NIMQ}) (Fig. 2*I*). Transgenic expression of wild-type *MCU* in the muscle of MCU^{52} mutant resulted in full recovery of mitochondrial Ca^{2+} uptake, as shown (Fig. 2, *D* and *E*). In contrast, expression of MCU^{NIMQ} failed to rescue the defective $[Ca^{2+}]_{mito}$ response of MCU^{52} mutant (Fig. 2, *J* and *K*). Therefore, the DIME motif is essential for its Ca^{2+} transport activity in *Drosophila* MCU.

EMRE is required for MCU activity in Drosophila

Eye-specific expression of MCU using *Gmr-Gal4* led to glazed phenotypes in the eye with partial loss of pigmentation

and irregular ommatidial array (Fig. 3*A*). The activity of MCU appeared critical for these effects because knockdown of MCU completely suppressed the eye phenotype (Fig. 3*A*). Consistently, a higher MCU expression with two copies of *UAS-MCU* transgene resulted in more severe phenotypes (Fig. 3*A*). Overexpression of EMRE, an essential component of the MCU complex, alone did not elicit defective phenotypes (Fig. 3*A*). Unexpectedly, co-expression of MCU and EMRE led to lethality. However, when those flies were reared at 23 °C instead of 25 °C, few managed to survive with defective eyes marked with black mass tissues, indicating that MCU and EMRE have a strong genetic interaction *in vivo* (Fig. 3*A*).

To confirm the role of EMRE in *Drosophila* MCU activity, we used the *UAS-EMRE RNAi* fly line to knock down EMRE expression. Silencing of EMRE led to impairment of mitochondrial Ca^{2+} uptake (Fig. 3, *B* and *C*), closely resembling the result obtained from MCU^{52} mutant (Fig. 2, *D* and *E*), implying that EMRE is required for mitochondrial Ca^{2+} uptake. Furthermore, expression of MCU in EMRE knockdown fly failed to increase the caffeine-induced $[Ca^{2+}]_{mito}$ response (Fig. 3, *B* and

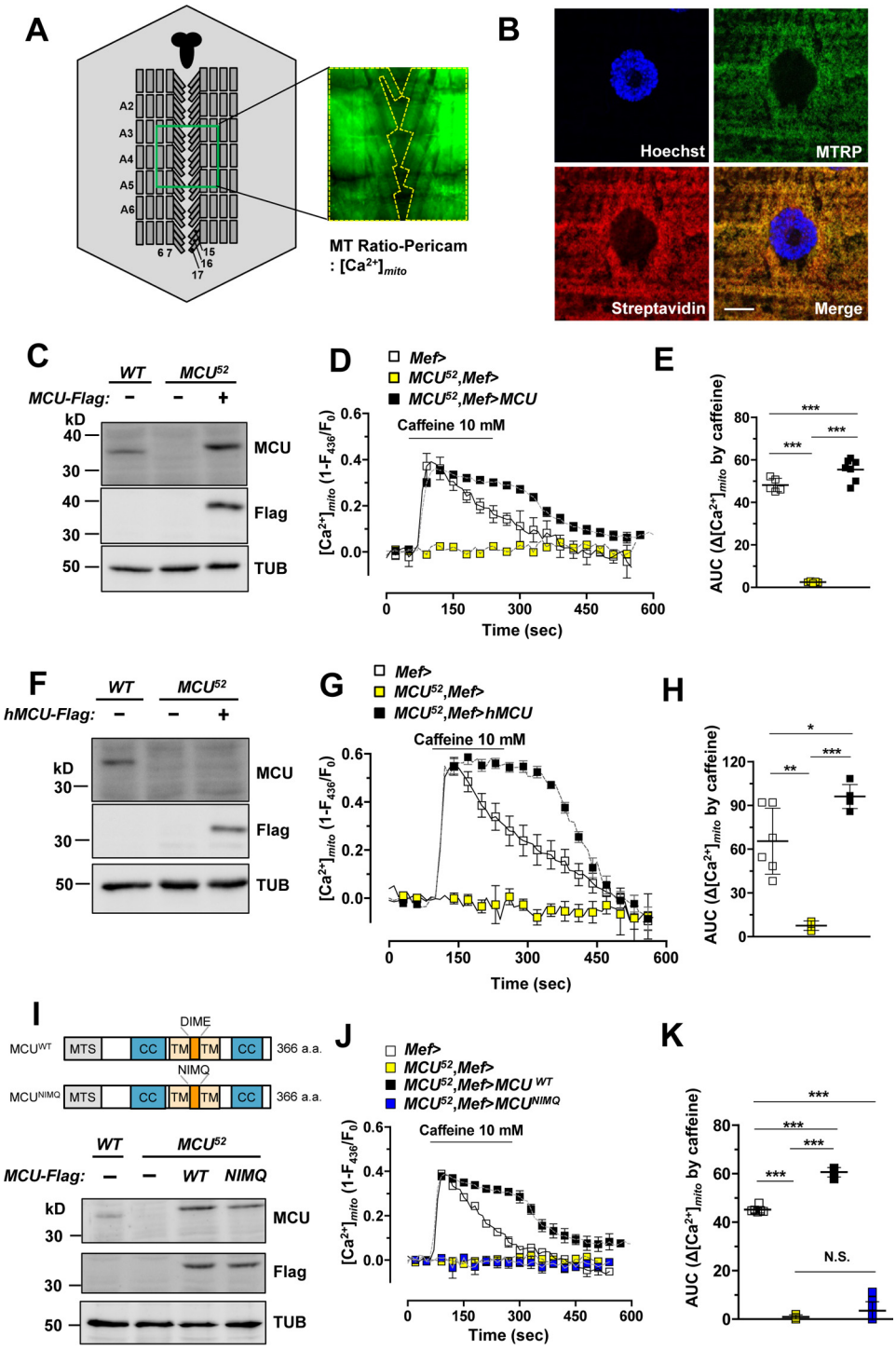

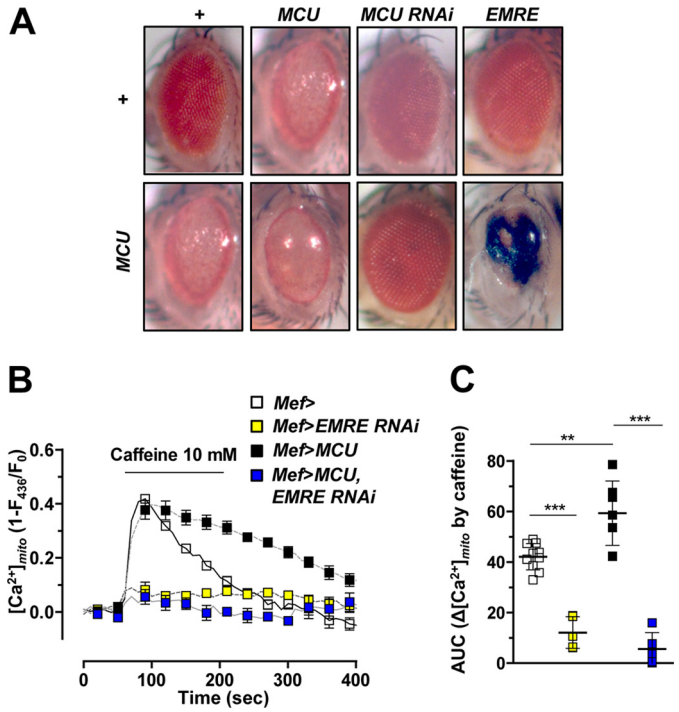

Figure 3. EMRE is required for MCU activity. *A*, eye-specific expression of transgenes using *Gmr-Gal4*. Severity of eye defect exacerbated as the level of *MCU* expression increased. Co-expression of MCU and EMRE in the eye led to lethality when reared in a 25 °C incubator. Several flies escaped the lethality when reared in a 23 °C incubator. The eye of an escaper fly is shown in the *right bottom panel*. All other flies were reared in a 25 °C incubator. From the *left top panel*, genotypes are as follows: *Gmr-Gal4/+*, *Gmr-Gal4/+;UAS-MCU-Myc/+*, *Gmr-Gal4/+;UAS-MCU RNAi/+*, *Gmr-Gal4/UAS-EMRE-FLAG*, *Gmr-Gal4/+;UAS-MCU-Myc/+*, *Gmr-Gal4/+;UAS-MCU-Myc/UAS-MCU-Myc*, *Gmr-Gal4/+;UAS-MCU RNAi/UAS-MCU-Myc*, and *Gmr-Gal4/UAS-EMRE-FLAG; UAS-MCU-Myc/+*. *B* and *C*, averaged traces (*B*) and quantitative analysis (*C*) of $[Ca^{2+}]_{mito}$ signals from the flies that express wild-type *MCU*, *EMRE RNAi*, or wild-type *MCU* and *EMRE RNAi* together ($n = 5–10$). Genotypes are as follows: *Mef-Gal4,UAS-MTRP/+* (*Mef>*), *UAS-EMRE RNAi/+;Mef-Gal4,UAS-MTRP/+* (*Mef>EMRE RNAi*), *UAS-MCU-FLAG/+;Mef-Gal4, UAS-MTRP/+* (*Mef>MCU*), and *UAS-EMRE RNAi/UAS-MCU-FLAG;Mef-Gal4,UAS-MTRP/+* (*Mef>MCU, EMRE RNAi*). ** and ***, $p < 0.01$ and $p < 0.001$, respectively. *Error bars*, S.D.

C). These results suggest that EMRE interacts with MCU genetically and is an essential and irreplaceable component for *Drosophila* MCU activity.

Loss of MCU provides resistance to oxidative stress

Oxidative stress is the most common pathogenic mediator for various diseases and is also involved in aging processes. To address whether mitochondrial Ca^{2+} uptake via MCU has any pathogenic role in inducing cell death under oxidative stress conditions, we first investigated the survival rates of wild-type fly and MCU^{52} mutant fed on hydrogen peroxide (H_2O_2)-containing food. Dihydroethidium (DHE) staining was used to detect the level of ROS in the thorax of flies. Elevated level of ROS was detected in the flies fed on 1% H_2O_2-containing food for the past 72 h, indicating that feeding H_2O_2 induced oxidative stress in the fly (supplemental Fig. S4*A*). Interestingly, MCU^{52} mutant flies survived significantly longer than wild-type flies when fed on 1% H_2O_2-containing food, whereas normal food caused the mutants to survive slightly less than wild-type flies. These results suggest that MCU^{52} mutant flies are more resistant to oxidative stress than wild-type flies (Fig. 4*A*).

To demonstrate whether ROS-induced apoptosis was attenuated by loss-of-function mutations of *MCU*, we performed a TUNEL assay under oxidative stress conditions. Wild-type flies showed strong TUNEL signals by 2% H_2O_2 treatment for 3 h, which was markedly reduced in MCU^{52} mutants (Fig. 4*B*). Additionally, we checked *hid5′F-WT*-GFP reporter expression and cleaved caspase-3 as a marker of early and late phases of apoptosis, respectively (41). Wild-type flies showed up-regulated GFP reporter expression from hid5′F-WT enhancer and increased cleaved caspase-3 staining, but MCU^{52} mutants displayed markedly reduced signals for both apoptotic markers (Fig. 4 (*C* and *D*) and supplemental Fig. S4 (*B* and *C*)). Consistently, we also confirmed the reduction of H_2O_2-induced apoptotic cell death by knockdown of *MCU* in *Drosophila* S2 cells (Fig. 4, *E* and *F*). Taken together, these results indicate that loss of MCU endows resistance to oxidative stress.

MCU-dependent Ca^{2+} uptake contributes to mitochondrial dysfunction by oxidative stress

To more clearly demonstrate whether oxidative stress can increase $[Ca^{2+}]_{mito}$ in *Drosophila*, we applied *tert*-butyl hydroperoxide (*t*-BuOOH) to larval muscle and applied H_2O_2 to S2 cells. First, in control larval muscle *in vivo*, $[Ca^{2+}]_{mito}$ was increased after treatment of *t*-BuOOH from 1 to 100 mM in a dose-dependent manner, suggesting that oxidative stress can increase $[Ca^{2+}]_{mito}$ (supplemental Fig. S5*A*). Compared with *in vitro* experiments, a higher dose of *t*-BuOOH is required to induce rapid oxidative stress on inner muscle tissue under the cuticle. Treatment of *t*-BuOOH (35 mM) on control flies

Figure 2. MCU regulates rapid mitochondrial calcium uptake. *A*, schematic representation of the muscle region of a dissected *Drosophila* larva to measure mitochondrial Ca^{2+} level. MTRP was expressed in larval muscle in *Mef>MTRP*. Fluorescence intensity was recorded from a well-focused region of body wall muscles 6, 7, 15, 16, and 17 of abdomen segments A2–A6. The central nervous system is marked with *solid black*. For simplicity, not all muscles and segments are shown. Fluorescence intensity from MTRP expressed in muscle was measured upon stimulation with 10 mM caffeine. *B*, mitochondrial localization of MTRP. *Green*, subcellular localization of MTRP in larval muscle. Hoechst (*blue*) and streptavidin (*red*) were used to mark DNA and mitochondria, respectively. The genotype is *Mef-Gal4/UAS-MTRP*. *Scale bar*, 10 μm. *C*, immunoblot analyses of endogenous MCU (*MCU*) and exogenously expressed FLAG-tagged MCU (*Flag*). *D–E*, averaged traces (*D*) and quantitative analysis (*E*) of $[Ca^{2+}]_{mito}$ signals after treatment of 10 mM caffeine from wild-type, MCU^{52}, and MCU^{52} mutant with exogenous *Drosophila* wild-type *MCU* expression ($n = 5–7$). Genotypes are as follows: *Mef-Gal4/UAS-MTRP* (*Mef>*), *Mef-Gal4,MCU^{52}/UAS-MTRP,MCU^{52}* (*MCU^{52},Mef>*), and *UAS-MCU-FLAG;Mef-Gal4,MCU^{52}/UAS-MTRP,MCU^{52}* (*MCU^{52},Mef>MCU*). *F*, immunoblot analyses of endogenous MCU (*MCU*) and exogenously expressed FLAG-tagged MCU (*Flag*). *G* and *H*, averaged traces (*G*) and quantitative analysis (*H*) of $[Ca^{2+}]_{mito}$ signals after treatment with 10 mM caffeine from wild type, MCU^{52}, and MCU^{52} mutant with human *MCU* expression ($n = 3–6$). Genotypes are as follows: *Mef-Gal4/UAS-MTRP* (*Mef>*), *Mef-Gal4,MCU^{52}/UAS-MTRP,MCU^{52}* (*MCU^{52},Mef>*), and *UAS-hMCU-FLAG;Mef-Gal4,MCU^{52}/UAS-MTRP,MCU^{52}* (*MCU^{52},Mef>hMCU*). *I–K*, a schematic representation of *Drosophila* wild-type *MCU* and MCU^{NIMQ} (*I*). *MTS*, mitochondrial targeting sequence; *CC*, coiled-coil domain; *TM*, transmembrane domain; *DIME*, DIME motif. Immunoblot analyses of endogenous MCU (*MCU*) and exogenously expressed FLAG-tagged MCU (*Flag*) are shown in the *bottom panels*. *J* and *K*, averaged traces (*J*) and quantitative analysis (*K*) of $[Ca^{2+}]_{mito}$ signals after 10 mM caffeine treatment from wild type, MCU^{52}, MCU^{52} mutant with *Drosophila* wild-type *MCU* overexpression, and MCU^{52} mutant with *Drosophila* MCU^{NIMQ} overexpression ($n = 4–10$). Genotypes are as follows: *Mef-Gal4/UAS-MTRP* (*Mef>*), *Mef-Gal4,MCU^{52}/UAS-MTRP,MCU^{52}* (*MCU^{52},Mef>*), *UAS-MCU-FLAG;Mef-Gal4,MCU^{52}/UAS-MTRP,MCU^{52}* (*MCU^{52},Mef>MCU^{WT}*), and *UAS-MCU^{NIMQ}-FLAG;Mef-Gal4,MCU^{52}/UAS-MTRP, MCU^{52}* (*MCU^{52},Mef>MCU^{NIMQ}*). *, **, and ***, $p < 0.05$, $p < 0.01$, and $p < 0.001$, respectively. *N.S.*, not significant. *Error bars*, S.D.

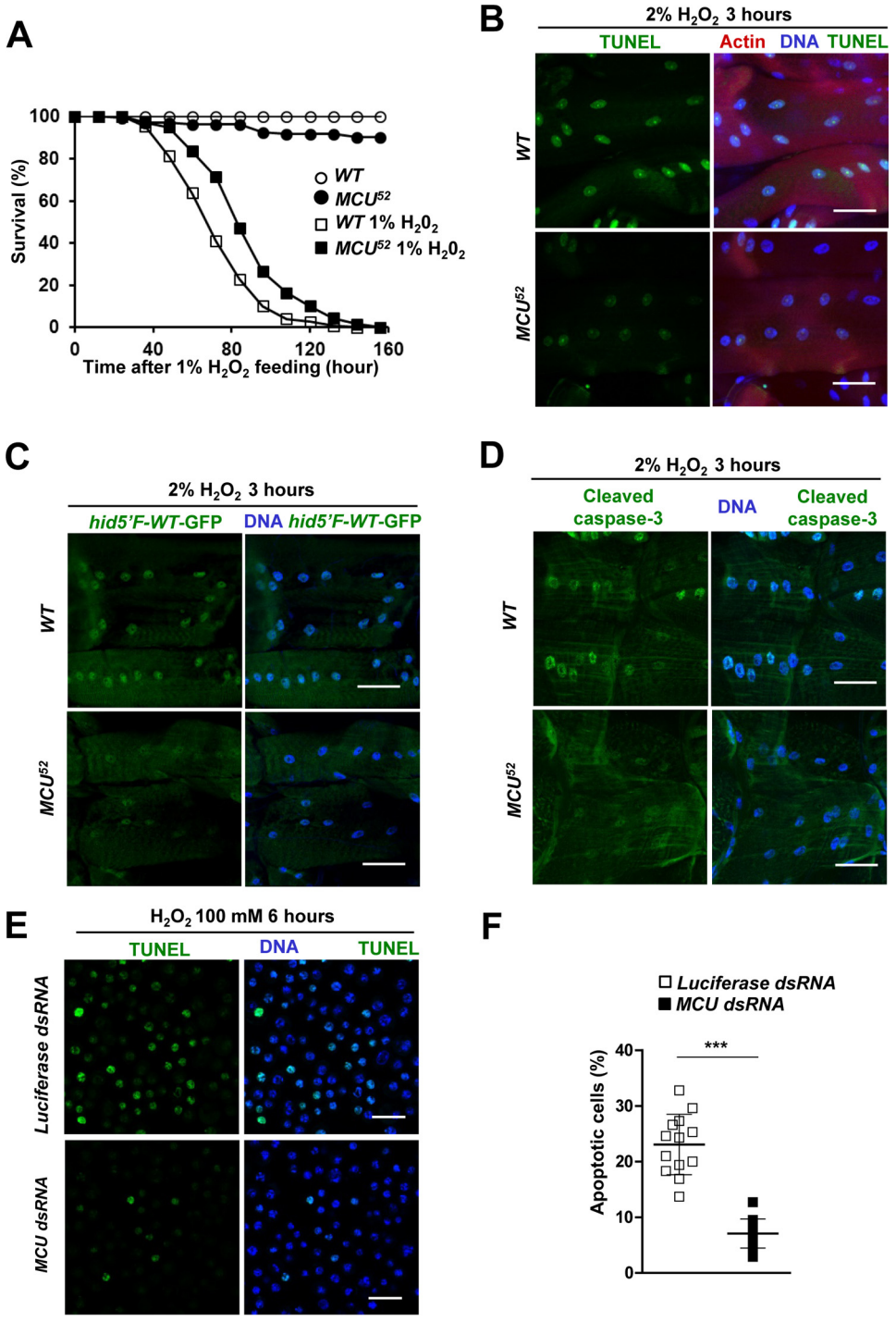

Figure 4. MCU mediates oxidative stress-induced apoptosis. *A*, survival curves of wild-type and *MCU*^{52} male flies on 1% H_2O_2-containing food (n = 133–149). Log-rank test: $p < 0.0001$. *B–D*, detecting apoptotic cells in larval muscle of wild-type and *MCU*^{52} flies after treatment of 2% H_2O_2 for 3 h. The assays were repeated >3 times. *B*, *left panels*, TUNEL signals; *right panels*, merged images of TUNEL (*red*), Hoechst (*blue*), and phalloidin (*green*) staining. *C*, *left panels*, GFP reporter expression from *hid5′F-WT* enhancer; *right panels*, *merged images* of GFP reporter (*green*) and Hoechst (*blue*) staining. Genotypes are WT (*hid5′F-WT-GFP/+*) and *MCU*^{52} (*hid5′F-WT-GFP/+;MCU*^{52}*/MCU*^{52}). *D*, *left panels*, cleaved caspase-3; *right panels*, *merged images* of cleaved caspase-3 (*green*) and Hoechst (*blue*) staining. *E*, TUNEL assays after treatment of 100 mM H_2O_2 for 6 h in S2 cells transfected with luciferase dsRNA or *Drosophila MCU* dsRNA. The TUNEL assay was repeated >3 times. *F*, the proportion of apoptotic nuclei in S2 cells transfected with luciferase dsRNA or *Drosophila MCU* dsRNA (n = 12–13). *Scale bars*, 50 μm (*B–D*) or 20 μm (*E*). ***, $p < 0.001$. *Error bars*, S.D.

(*Mef*>) markedly increased $[Ca^{2+}]_{mito}$ (Fig. 5*A*). As expected, the $[Ca^{2+}]_{mito}$ response induced by *t*-BuOOH was abolished in *MCU*^{52} mutant (*MCU*^{52},*Mef*>), demonstrating the critical role of MCU in oxidative stress-induced $[Ca^{2+}]_{mito}$ increase (Fig. 5, *A* and *B*). Transgenic expression of *Drosophila* MCU (*MCU*^{52},*Mef*>*MCU*) rescued the abolished $[Ca^{2+}]_{mito}$ response in *MCU*^{52} mutant (*MCU*^{52},*Mef*>) (Fig. 5, *A* and *B*). By contrast, the $[Ca^{2+}]_i$ changes induced by *t*-BuOOH were not significantly different between control (*Mef*>) and *MCU*^{52} mutant (supplemental Fig. S5*B*). We also detected $[Ca^{2+}]_{mito}$

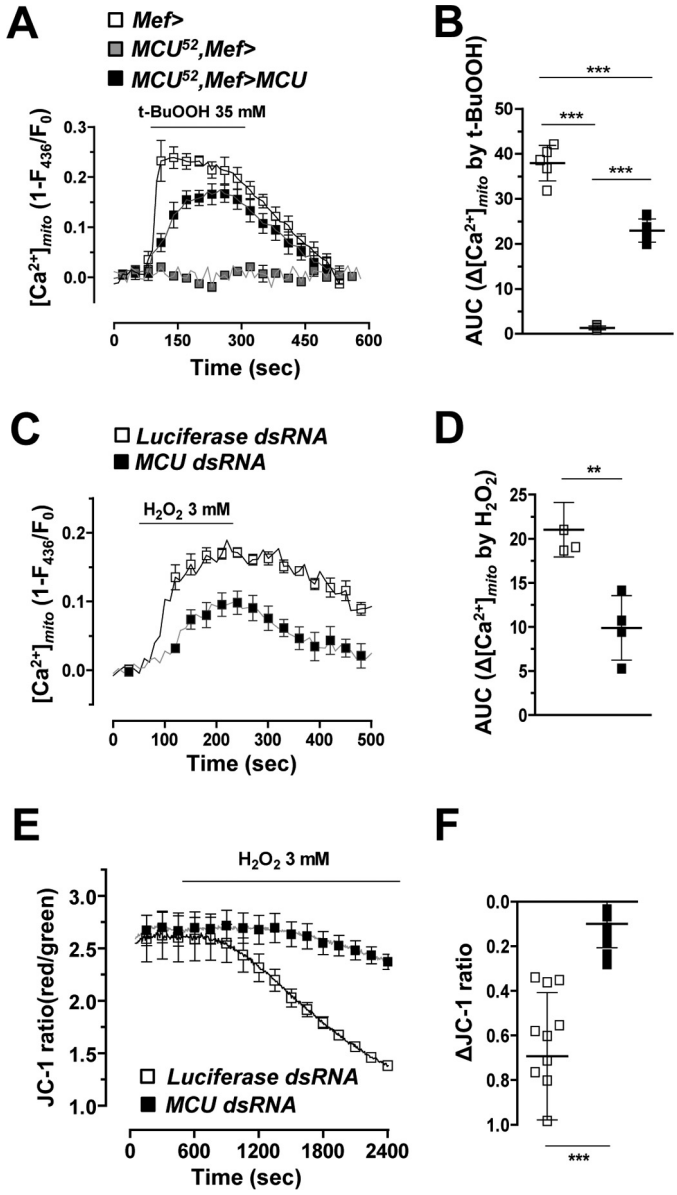

Figure 5. MCU is required for oxidative stress-induced mitochondrial calcium uptake. *A* and *B*, averaged traces (*A*) and quantitative analysis (*B*) of $[Ca^{2+}]_{mito}$ signals after 35 mM *t*-BuOOH treatment from wild-type, *MCU*^{52}, and *MCU*^{52} mutant with wild-type *Drosophila MCU* expression ($n = 4–7$). Genotypes are as follows: *Mef-Gal4/UAS-MTRP* (*Mef*>), *Mef-Gal4,MCU*^{52}*/UAS-MTRP-,MCU*^{52} (*MCU*^{52}*,Mef*>), and *UAS-MCU-FLAG/+;Mef-Gal4,MCU*^{52}*/UAS-MTRP-,MCU*^{52} (*MCU*^{52}*,Mef>MCU*). *C* and *D*, averaged traces (*C*) and quantitative analysis (*D*) of $[Ca^{2+}]_{mito}$ signals after 3 mM H_2O_2 treatment from S2 sells transfected with luciferase dsRNA or *Drosophila MCU* dsRNA ($n = 4$). *E*, measurement of Ψ_{mito} using JC-1 in S2 cells transfected with luciferase dsRNA or *MCU* dsRNA upon 3 mM H_2O_2 treatment. *F*, quantitative analysis of *E* ($n = 12–16$). ** and ***, $p < 0.01$, and $p < 0.001$, respectively. *Error bars*, S.D.

rise in S2 cells upon H_2O_2 stimulation (Fig. 5*C*). Consistent with the *in vivo* muscle data, *MCU* dsRNA-treated S2 cells showed reduced H_2O_2-induced mitochondrial Ca^{2+} uptake (−63%) in comparison with control (*Luciferase dsRNA-treated*) (Fig. 5, *C* and *D*). To estimate the functional deterioration of mitochondria as a result of $[Ca^{2+}]_{mito}$ overload, we monitored mitochondrial membrane potential (Ψ_{mito}) by using potential-sensitive JC-1 dye. Oxidative stress by H_2O_2 treatment (3 mM) elicited depolarization of Ψ_{mito} in S2 cells (Fig. 5*E*). Intriguingly, knockdown of *MCU* strongly prevented H_2O_2-induced $\Delta\Psi_{mito}$ collapse in S2 cells (Fig. 5, *E* and *F*). Based on these results, we suggest that mitochondrial dysfunction and apoptotic cell death induced by oxidative stress are related to MCU-mediated $[Ca^{2+}]_{mito}$ overload.

IP_3R and MCU participate in oxidative stress-induced ER–mitochondria Ca^{2+} transfer

Oxidative stress is reported to activate IP_3R, a Ca^{2+} channel in the ER, resulting in ER Ca^{2+} release (33, 34). Released Ca^{2+} from the ER provides high Ca^{2+} level in microdomains of ER-mitochondrial junction called MAM. IP_3R is a component of tethering structure between the ER and mitochondria (31). Therefore, we investigated the involvement of IP_3R in ER-mitochondria Ca^{2+} transfer under oxidative stress.

Muscle-specific expression of exogenous *MCU* using *Mef-Gal4* was lethal in pupa stage of the transgenic fly (Fig. 6*A*). However, this lethality was blocked by knockdown of IP_3R, suggesting that MCU and IP_3R have a strong genetic interaction *in vivo* (Fig. 6*A*). To confirm the role of IP_3R in mitochondrial Ca^{2+} uptake, we compared $[Ca^{2+}]_{mito}$ increase induced by oxidative stress between control (*Mef*>) and muscle-specific *IP_3R* knockdown flies (*Mef>IP_3R RNAi*). The *IP_3R* knockdown flies showed significantly reduced mitochondrial Ca^{2+} uptake (−41.2%) upon *t*-BuOOH stimulation in comparison with control (*Mef*>) (Fig. 6, *B* and *C*). Additionally, when we silenced *IP_3R* in *MCU* transgenic flies (*Mef>MCU*, *IP_3R RNAi*), the $[Ca^{2+}]_{mito}$ induced by *t*-BuOOH was reduced by 34.7% when compared with that of *Mef>MCU* flies (Fig. 6, *B* and *C*). This was consistent with our previous results, where knockdown of *IP_3R* blocked the lethality induced by MCU overexpression (Fig. 6*A*). In S2 cells, H_2O_2-induced $[Ca^{2+}]_{mito}$ increase was also strongly inhibited (−64.0%) by transfection of *IP_3R* dsRNA (Fig. 6, *D* and *E*). These results strongly indicate that both IP_3R and MCU are critical for the Ca^{2+} transfer from the ER to mitochondria.

Finally, we examined the involvement of IP_3R and MCU in oxidative stress-induced toxicity using transgenic flies that overexpress or silence superoxide dismutase 1 (*Sod1*). First, the degenerated eye phenotype in the flies expressing MCU using *Gmr-Gal4* driver, as shown in Fig. 3*A*, was restored by *Sod1* expression but was exacerbated by *Sod1* knockdown (Fig. 6*F*). As stated above, the lethality of MCU overexpression using *Mef-Gal4* was prevented by the knockdown of IP_3R (Fig. 6*A*). However, interestingly, simultaneous knockdown of both *Sod1* and *IP_3R* failed to rescue the lethal phenotype of MCU overexpression using *Mef-Gal4* (Fig. 6*G*). These results suggest that endogenous ROS plays an imperative role in the IP_3R- and MCU-mediated mitochondrial Ca^{2+} overload and toxicity.

Discussion

In this study, we established a *Drosophila* model system to understand functional roles of MCU in mitochondrial Ca^{2+} homeostasis *in vivo*. By generating and characterizing a null mutant of *MCU* (*MCU*^{52}), we investigated the physiological roles of MCU in *Drosophila*. *MCU*^{52} mutant did not show significant changes in body weight, metabolism, and autophagic flux compared with wild-type flies. However, caffeine-induced $[Ca^{2+}]_{mito}$ increase was abolished in *MCU*^{52} mutant larval

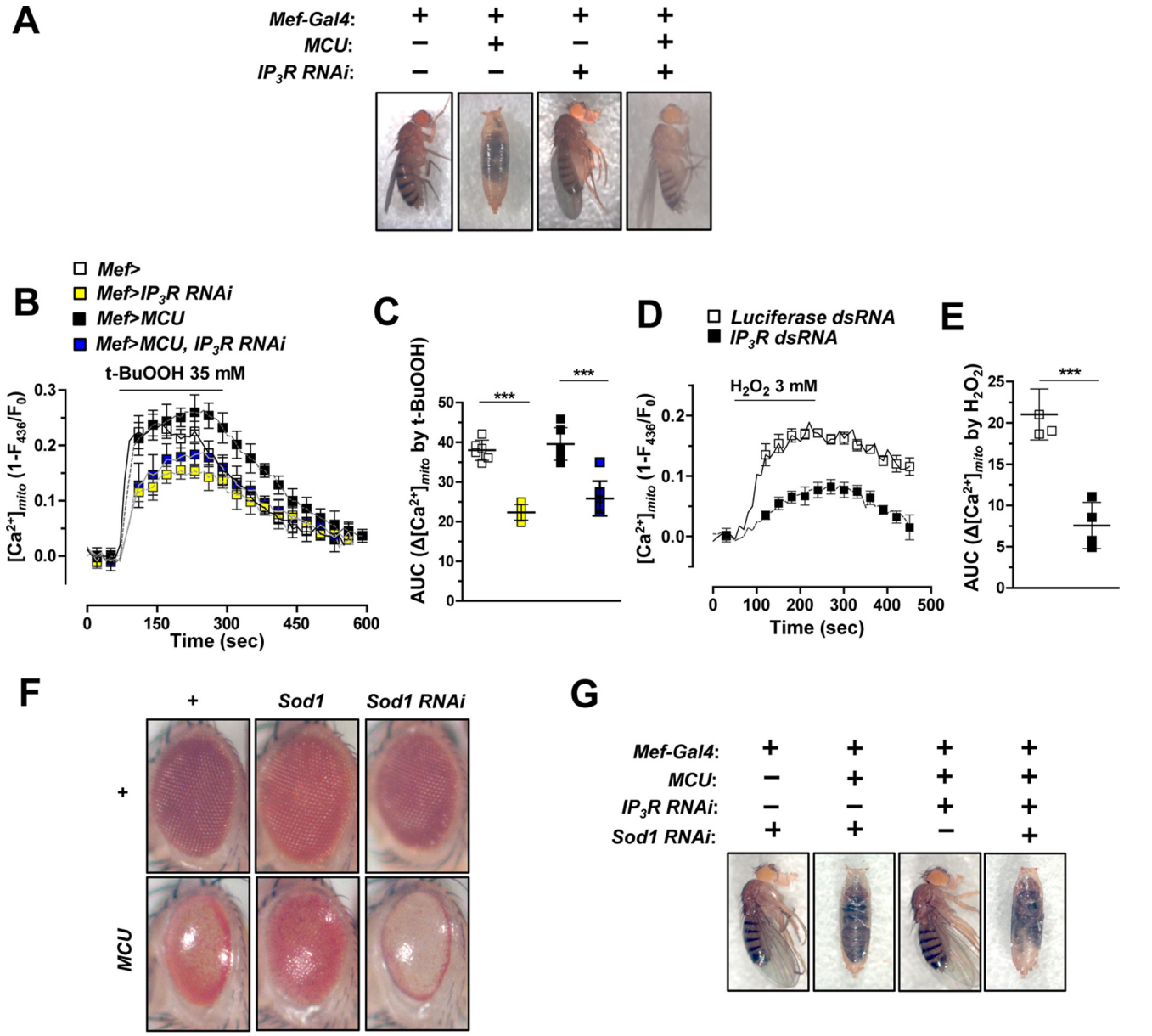

Figure 6. MCU is required for oxidative stress-induced mitochondrial calcium uptake. *A*, knockdown of IP_3R blocked the lethality induced by MCU overexpression in muscle. Genotypes are as follows: *Mef-Gal4/+*, *UAS-MCU-FLAG/+;Mef-Gal4/+*, *Mef-Gal4/UAS-IP$_3$R RNAi*, and *UAS-MCU-FLAG/+;Mef-Gal4/UAS-IP$_3$R RNAi*. *B* and *C*, averaged traces (*B*) and quantitative analysis (*C*) of $[Ca^{2+}]_{mito}$ signals from the flies that express *IP$_3$R* RNAi, *Drosophila MCU*, or *Drosophila MCU* and *IP$_3$R* RNAi upon treatment with 35 mM *t*-BuOOH ($n = 5–9$). Genotypes are as follows: *Mef-Gal4,UAS-MTRP/+* (*Mef>*), *Mef-Gal4,UAS-MTRP/UAS-IP$_3$R RNAi* (*Mef> IP$_3$R RNAi*), *UAS-MCU-FLAG/+;Mef-Gal4,UAS-MTRP/+* (*Mef>MCU*), and *UAS-MCU-FLAG/+;Mef-Gal4, UAS-MTRP/UAS-IP$_3$R RNAi* (*Mef>MCU, IP$_3$R RNAi*). *D* and *E*, averaged traces (*D*) and quantitative analysis (*E*) of $[Ca^{2+}]_{mito}$ signals from S2 sells transfected with luciferase dsRNA or *IP$_3$R* dsRNA upon treatment with 3 mM H_2O_2 ($n = 4$). *F*, eye-specific expression of transgenes using *Gmr-Gal4*. In clockwise order from the *top left panel*, genotypes are as follows: *Gmr-Gal4/+*, *Gmr-Gal4/UAS-Sod1*, *Gmr-Gal4/UAS-Sod1 RNAi*, *Gmr-Gal4/UAS-Sod1 RNAi;UAS-MCU-Myc/+*, *Gmr-Gal4/UAS-Sod1;UAS-MCU-Myc/+*, and *Gmr-Gal4/+;UAS-MCU-Myc/+*. *G*, genetic interactions among *MCU*, *IP$_3$R*, and *Sod1*. Genotypes are as follows from *left* to *right*: *UAS-Sod1 RNAi/+;Mef-Gal4/+*, *UAS-MCU-FLAG/UAS-Sod1 RNAi;Mef-Gal4/+*, *UAS-MCU-FLAG/+;Mef-Gal4/UAS-IP$_3$R RNAi*, and *UAS-MCU-FLAG/UAS-Sod1 RNAi;Mef-Gal4/UAS-IP$_3$R RNAi*. ***, $p < 0.001$. *Error bars*, S.D.

muscle, which was completely rescued by transgenic expression of either human or *Drosophila MCU*. In addition, the DIME amino acid motif, which forms the ion selectivity filter of the MCU channel, was indispensable for the activity of *Drosophila* MCU, suggesting that MCU is evolutionarily highly conserved. In *MCU^{52}* mutant larval muscle and *MCU*-silenced S2 cells, exogenous ROS-induced $[Ca^{2+}]_{mito}$ increase, $\Delta\Psi_{mito}$ dissipation, and cell death were prevented. Suppression of IP_3R, which is a Ca^{2+} release channel in the ER, also protects from ROS-mediated mitochondrial Ca^{2+} overload and cytotoxicity. These results demonstrate the critical role of *Drosophila* MCU in Ca^{2+} transfer from the ER to mitochondria, contributing to oxidative stress-induced mitochondrial dysfunction and apoptotic cell death.

Mitochondrial Ca^{2+} is a crucial regulator in energy metabolism, Ca^{2+} sequestration, and cell death. However, our *Drosophila MCU* loss-of-function mutant did not exhibit significant metabolic phenotypes. These unexpected results can be explained by undefined compensatory mechanisms for mitochondrial Ca^{2+} uptake, such as MCU-independent slow Ca^{2+}

channels or exchangers. It is also conceivable that rapid changes in $[Ca^{2+}]_{mito}$ via MCU may not be required for maintaining basal metabolism and daily activities in *Drosophila* except for exogenous stress or emergency crisis. Mouse *MCU* knock-out models with outbred CD1 background also did not show any significant phenotypes except for reduced abilities to perform strenuous work (20). However, strangely, *MCU* deletion within a C57BL/6 background resulted in embryonic lethality (42). This discrepancy suggests that a compensatory mechanism that is absent in C57BL/6 background exist in CD1 mice and allows MCU-independent mitochondrial Ca^{2+} uptake during animal development. By contrast, up-regulation of MCU augments mitochondrial Ca^{2+} uptake, leading to aberrantly high $[Ca^{2+}]_{mito}$ level, and this stress accelerates further superoxide production through activation of the electron transport chain or other mechanisms. Together with increased $[Ca^{2+}]_{mito}$ and oxidative stress in mitochondrial matrix, this facilitates opening of mPT and cytochrome *c* release, leading to apoptotic cell death. In our study, ectopic overexpression of MCU in *Drosophila* muscle led to pupal lethality (Fig. 6*A*). Additionally, MCU overexpression in *Drosophila* eye using *Gmr-Gal4* driver resulted in severely destroyed ommatidial array (Fig. 3*A*). These results imply that overexpression of *Drosophila* MCU accelerates mitochondrial Ca^{2+} overload that is detrimental to various tissues and ultimately impairs a viability of organism.

EMRE is an essential auxiliary subunit containing a mitochondrial targeting sequence at its N terminus, a single transmembrane domain located at inner mitochondrial membrane, and an aspartate-rich C terminus (12). The MCU complex requires EMRE for its reconstitution in mammalian cells, but not in *Dictyostelium discoideum* (43). In mammalian cells, suppression of EMRE abrogates MCU-mediated Ca^{2+} currents demonstrated by mitoplast patch clamp experiment (12, 14). However, functional consequences of EMRE overexpression have not been studied yet (44). In our study, EMRE showed a strong genetic interaction with MCU in *Drosophila*. Co-expression of *Drosophila* EMRE and MCU in fly muscle led to lethality in larva stage. Furthermore, depletion of EMRE in larval muscle abolished caffeine-induced $[Ca^{2+}]_{mito}$ increase regardless of the expression level of MCU, indicating that EMRE is required for MCU activity from human to *Drosophila*.

Recent studies reported that MCU is involved in Ca^{2+} excitotoxicity of cortical neurons (26) and oxidative stress-induced cell death of primary cerebellar granule neurons (45). Oxidative stress is proposed as the main causative factor for neurodegenerative, cardiovascular, and other mitochondria-related diseases (46). Previous studies reported that oxidative stress increases $[Ca^{2+}]_i$ (47–49), although there are controversies whether the source of Ca^{2+} is from the extracellular environment or intracellular stores. We observed marked and sustained $[Ca^{2+}]_{mito}$ rises by exogenous oxidative stress inducers, such as H_2O_2 and *t*-BuOOH in *Drosophila*, which have not been investigated previously. Oxidative stress produced by endoplasmic reticulum oxidase 1α (ERO1α) can stimulate Ca^{2+} release from the ER by activating IP_3R (33). Loss of Ca^{2+} store in the ER by ROS induces ER stress due to impaired Ca^{2+}-sensitive chaperone activities and further ROS production by induction of C/EBP homologous protein (33). In addition, depletion of Ca^{2+} in the ER stimulates Ca^{2+} influx from outside of the cell via store-operated Ca^{2+} entry (50). Both Ca^{2+} release from the ER and influx from extracellular environment burden cells with the pathology of mitochondrial Ca^{2+} overload.

Our study clearly showed that loss-of-function mutation of MCU abrogated $[Ca^{2+}]_{mito}$ increases triggered by *t*-BuOOH in fly muscle. Moreover, knockdown of IP_3R also significantly attenuated oxidative stress-induced $[Ca^{2+}]_{mito}$ rises, which explains the protective roles of IP_3R RNAi against lethality in MCU-overexpressed flies (Fig. 6*A*). Oxidative stress can increase ER Ca^{2+} release by activating not only IP_3R but also ryanodine receptor (RyR), both of which are main Ca^{2+} release channels in the ER (33, 51). Although it has been known that RyR plays more important roles than IP_3R in Ca^{2+} release from the sarcoplasmic reticulum in skeletal muscle, the muscle tissues from larva, pupa, and adult *Drosophila* express IP_3R, which is critical for the muscle development (52). In this study, we could not investigate the interaction between RyR and MCU for oxidative stress-induced mitochondrial Ca^{2+} overload and lethality because all of the flies with muscle-specific knockdown of *RyR* died before larval stage. However, we still consider that RyR is another strong candidate involved in mitochondrial Ca^{2+} overload by oxidative stress in muscle.

In summary, we have established a *Drosophila* system to study the MCU complex *in vivo*, demonstrating that oxidative stress induces Ca^{2+} release from the ER and mitochondrial Ca^{2+} uptake via MCU, resulting in mitochondrial dysfunction and cell death *in vivo*. Intriguingly, a recent study showed that ROS modifies MCU directly by *S*-glutationylation and consequently influences the channel activity of MCU (53). These pieces of evidence indicate both direct and indirect regulation of the Ca^{2+} channel activity of MCU by ROS. Further genetic studies would enable us to discover novel relationships connecting mitochondrial Ca^{2+} homeostasis and other cellular activities. In addition, studying the *in vivo* role of MCU and its related genes in *Drosophila* will further extend our knowledge of their pathophysiological significance.

Experimental procedures

Fly strains

MCU^{52} mutant and a revertant were generated using P-element excision of the GS11565 line obtained from the Kyoto Stock Center (Kyoto Institute of Technology, Kyoto, Japan). The revertant with a precise P-element excision was used as a wild-type control. The P-element excisions in *MCU*^{52} and the revertant flies were confirmed by PCR using a primer set of the following sequences: 5′-GACGGAATTGCGATGGAAAATC-3′ and 5′-GCCAAAAATCCCATTCTAGTG-3′. The *MCU* cDNA clone LD26402 and the *EMRE* cDNA clone RE55001 were purchased from the *Drosophila* Genomics Resource Center (Indiana University, Bloomington, IN). *UAS-MCU-FLAG*, *UAS-hMCU-FLAG*, *UAS-MCU*^{NIMQ}*-FLAG*, and *UAS-EMRE-FLAG* were generated by microinjection of pUAST vector-cloned DNA into *w*^{1118} embryos. *Cg-Gal4*, *Mef-Gal4*, *Gmr-Gal4*, and *UAS-GCaMP3.T* were obtained from the Bloomington *Drosophila* Stock Center (Indiana University,

Bloomington, IN). *UAS-MCU RNAi* (v9501), *UAS-IP$_3$R RNAi* (v6484), and *UAS-EMRE RNAi* (v104493) were provided by the Vienna *Drosophila* RNAi Center (Vienna, Austria). Other flies were provided with generosity: *UAS-MTRP* from Dr. G. T. Macleod (University of Texas Health Science Center, San Antonio, TX); *UAS-mCherry-ATG8a* from Dr. T. P. Neufeld (University of Minnesota, Minneapolis, MN); *UAS-MCU-Myc* from Dr. S. B. Lee (DGIST, Daegu, Korea); and *hid5′F-WT-GFP* from Dr. W. Du (University of Chicago).

Quantitative RT-PCR

Wandering larvae were collected, and total RNA was extracted using TRIzol reagent (Invitrogen). Extracted RNAs were reverse transcribed by Moloney murine leukemia virus reverse transcriptase (Promega) and amplified by PCR with primer sets of the following sequences: 5′-GTCTCGCCCT-GCGTTTGG-3′ and 5′-CGAAGCTTCTGTGCTGCTG-3′ for *MCU* and 5′-GCGCTTCTTGGAGGAGACGCCG-3′ and 5′-GCTTCAACATGACCATCCGCCC-3′ for *RP49*. *MCU* mRNA levels were normalized by *RP49* mRNA levels.

Immunoblotting analysis

For immunoblot samples, tissues were homogenized in ice-cold lysis buffer (20 mM Tris-Cl, pH 7.5, 100 mM NaCl, 1 mM EDTA, 2 mM EGTA, 1 mM Na_2VO_4, 50 mM β-glycerol phosphate, 50 mM NaF, and 1% Triton X-100). Homogenized samples were incubated in ice for 15 min, centrifuged, and denatured. Rabbit anti-FLAG antibody (Cell Signaling Technology), mouse anti-*Drosophila* MCU polyclonal antibody (epitope: EDGETDKHKKPTTG) (AbClon), mouse anti-β tubulin antibody (DSHB), and anti-porin antibody (54) were used in immunoblot analyses.

Food intake assay

To measure feeding activity for 24 h, the food intake assay was conducted as described previously (55).

Measurement of trehalose and glucose

Trehalose and glucose in fly body fluid were measured as described previously (56). For each genotype, hemolymph from 5–7 wandering larvae was extracted by tearing up the cuticles. 1 μl of hemolymph was diluted with 99 μl of trehalase buffer (5 mM Tris, pH 6.6, 137 mM NaCl, and 2.7 mM KCl) and incubated at 70 °C for 5 min. Then 40 μl of diluted hemolymph was mixed with either 40 μl of trehalase buffer or 40 μl of trehalase solution. Trehalase solution was prepared by diluting 3 μl of porcine trehalase (Sigma) in 1 ml of trehalase buffer. Samples were incubated at 37 °C overnight, and glucose levels were measured using a glucose assay kit (Sigma-Aldrich).

Starvation-induced autophagy assay

Third instar larvae before wandering stage were rinsed with PBS and either starved in a double-distilled water–containing Petri dish or fed in a food-containing vial for 4 h. Then larvae were dissected and fixed in 4% paraformaldehyde. mCherry-ATG8a signals in larval fat body were observed under a confocal microscope.

Survival curves on H_2O_2-containing food

120–130 3–5-day-old males were starved 4–6 h in double-distilled water–containing vials and transferred to vials containing either 1% H_2O_2 or 5% sucrose. Surviving flies were counted every 12 h.

TUNEL assay

To detect H_2O_2-induced cell death, wandering larvae were dissected and incubated for 3 h in Schneider's medium containing 2% H_2O_2. Dissected larvae were fixed in 4% paraformaldehyde (PFA) and washed with PBS. Samples were incubated in 0.1 M sodium citrate at 65 °C, and cell death was detected using an *in situ* cell death detection kit (Roche Applied Science). After TUNEL reaction, the samples were stained by phalloidin and Hoechst to detect filamentous actin and nucleus, respectively. To detect in S2 cells, S2 cells were incubated for 6 h in Schneider's medium-containing 100 mM H_2O_2. After fixation with 4% PFA for 15 min and washing with PBS, cells were incubated in 0.1 M sodium citrate at room temperature for 10 min, and apoptosis was detected by using an *in situ* cell death detection kit (Roche Applied Science).

Immunostaining

Third instar larvae were dissected and incubated for 3 h in Schneider's medium containing 2% H_2O_2. Then samples were fixed in 4% PFA PBST (0.1% Triton X-100 in PBS) for 30 min and washed with PBST. The samples were blocked with 5% FBS, 0.5% BSA PBST (blocking buffer) for 1 h and then incubated with primary antibodies overnight at 4 °C. After three washes for 10 min in blocking buffer, the samples were treated with secondary antibodies and Hoechst 33258 (Invitrogen) in blocking buffer for 45 min. After extensive washes, samples were placed in mounting medium. Primary antibodies used in this study were as follows: anti-GFP rabbit monoclonal antibody (1:500; Thermo Fisher Scientific, A11222) and anti-cleaved caspase-3 polyclonal antibody (1:200; Cell Signaling Technology, 9661). Alexa Fluor 568 streptavidin (Thermo Fisher Scientific) and anti-ATP5a mouse monoclonal antibody (Abcam, ab14748) were used to detect mitochondria. Fluorescein-conjugated F(ab′)$_2$ fragment goat anti-rabbit IgG (Jackson ImmunoResearch, 111-096-144) and rhodamine red-X–conjugated F(ab′)$_2$ fragment goat anti-mouse IgG (Jackson ImmunoResearch, 115-296-146) were used as secondary antibodies.

DHE staining

For ROS detection, adult fly thoraces were dissected in Schneider's medium, incubated for 5 min with 30 μM DHE in the same medium, washed twice, fixed slightly with 4% PFA for 8 min, and rinsed with PBS.

Drosophila S2 cell culture and dsRNA bathing

Drosophila S2-DRSC cells were cultured and dsRNA bathing was conducted as described previously (57). For silencing mRNA expression of *MCU* and *IP$_3$R*, dsRNA was synthesized and bathed. The following primers were used for dsRNA synthesis: *MCU* dsRNA, 5′-TAATACGACTCACTATAGGGTG-GAGGATGTGAAGAATCGC-3′ and 5′-TAATACGACT-

CACTATAGGGTGAATCGTCCAACTGTGGCT-3′; *IP$_3$R* dsRNA, 5′-TAATACGACTCACTATAGGGCGTTGCTTTATCCTTTGCCA-3′ and 5′-TAATACGACTCACTATAGGGCCGCATAGAGGGACACAATG-3′; luciferase dsRNA, 5′-TAATACGACTCACTATAGGGAGAGGCCCGGCGCCATTCTATC-3′ and 5′-TAATACGACTCACTATAGGGAGAGATTGGGAGCTTTTTTTGCACG-3′. After 4 days of dsRNA bathing, S2 cells were used for a TUNEL assay or fluorescence measurement.

Measurement of mitochondrial matrix or cytosolic calcium

To measure $[Ca^{2+}]_{mito}$ in larval muscle, MTRP was expressed by *Mef-Gal4* and *UAS-MTRP*. Wandering third instar larvae were dissected as described previously (58) with some modifications. Larvae were dissected in perfusion buffer (2 mM $CaCl_2$, 4 mM $MgCl_2$, 2 mM KCl, 2 mM NaCl, 5 mM HEPES, 35.5 mM sucrose, 7 mM L-glutamic acid, pH 7.3, with NaOH) on a stereomicroscope and transferred to a confocal microscope. Transferred larvae were perfused with the same buffer, and fluorescence images were acquired by using an inverted microscope (IX-81, Olympus, Tokyo, Japan) with an array laser confocal spinning disk (CSU10, Yokogawa Electric Corp., Tokyo, Japan) and a cooled charge-coupled device camera (Cascade 512B, Photometrics, Tucson, AZ). Acquired fluorescence images from 435-nm excitation (Ex) and 535-nm emission (Em) were analyzed using Metafluor 6.3 software (Universal Imaging, Molecular Devices) (11). Cytosolic Ca^{2+} level ($[Ca^{2+}]_i$) was measured by using the confocal system (488-nm Ex/535-nm Em) in GCaMP3-expressed larval muscle (59). To measure $[Ca^{2+}]_{mito}$ in S2 cells, we used a mitochondria-targeted ratio-pericam plasmid (RPmit4.1), generously provided by Dr. Roger Tsien (University of California, San Diego, CA). Cells were transfected with siRNA for 24 h and then transfected with RPmit4.1 using X-tremeGENE (Roche Diagnostics GmbH, Mannheim, Germany). After 48 h of RPmit4.1 transfection, cells were perfused with KRB solution (140 mM NaCl, 3.6 mM KCl, 0.5 mM NaH_2PO_4, 0.5 mM $MgSO_4$, 1.5 mM $CaCl_2$, 10 mM HEPES, 2 mM $NaHCO_3$, 5.5 mM glucose, pH 7.4, titrated with NaOH), and fluorescence images (435-nm Ex/535-nm Em) were acquired.

Calculation of $[Ca^{2+}]_{mito}$ increases

In every scattered plot, the *y* axis represents area under the curve of the $[Ca2^{+}]_{mito}$ imaging result under caffeine, *t*-BuOOH, or H_2O_2 treatment.

Measurement of mitochondrial membrane potential

To measure the mitochondrial membrane potential (Ψ_{mito}), S2 cells seeded onto black-walled 96-well plates (1.2×10^5 cells/well) were loaded with a lipophilic cationic dye, JC-1 (1.5 μM), for 30 min. Cells were washed with KRB solution, and JC-1 fluorescence intensities of red (540-nm Ex/590-nm Em; J-aggregates) and green (490-nm Ex/540-nm Em; monomer) were measured ratiometrically at room temperature using a multiwell fluorescence reader (Flex-Station, Molecular Devices) (60).

Statistics

Values are presented as mean ± S.D., and *n* is the number of independent experiments. *p* values were obtained by Student's *t* test or one-way analysis of variance, and <0.05 was considered to be significant.

Author contributions—S. C., K.-S. P., and J. C. conceived and designed the experiments; S. C., X. Q., S. B., H. Y., and J. K. performed the experiments; K.-S. P. and J. C. analyzed the data; and S. C., J. K., S. B., J. P., K.-S. P., and J. C. wrote the paper.

Acknowledgments—We thank Drs. Gregory T. Macleod, Thomas P. Neufeld, Sung-Bae Lee, and Wei Du for providing Drosophila stocks. We are grateful to the Bloomington Stock Center and the Vienna Drosophila RNAi Center.

References

1. Kirichok, Y., Krapivinsky, G., and Clapham, D. E. (2004) The mitochondrial calcium uniporter is a highly selective ion channel. *Nature* **427,** 360–364
2. Baughman, J. M., Perocchi, F., Girgis, H. S., Plovanich, M., Belcher-Timme, C. A., Sancak, Y., Bao, X. R., Strittmatter, L., Goldberger, O., Bogorad, R. L., Koteliansky, V., and Mootha, V. K. (2011) Integrative genomics identifies MCU as an essential component of the mitochondrial calcium uniporter. *Nature* **476,** 341–345
3. De Stefani, D., Raffaello, A., Teardo, E., Szabò, I., and Rizzuto, R. (2011) A forty-kilodalton protein of the inner membrane is the mitochondrial calcium uniporter. *Nature* **476,** 336–340
4. Oxenoid, K., Dong, Y., Cao, C., Cui, T., Sancak, Y., Markhard, A. L., Grabarek, Z., Kong, L., Liu, Z., Ouyang, B., Cong, Y., Mootha, V. K., and Chou, J. J. (2016) Architecture of the mitochondrial calcium uniporter. *Nature* **533,** 269–273
5. Lee, S. K., Shanmughapriya, S., Mok, M. C. Y., Dong, Z., Tomar, D., Carvalho, E., Rajan, S., Junop, M. S., Madesh, M., and Stathopulos, P. B. (2016) Structural insights into mitochondrial calcium uniporter regulation by divalent cations. *Cell Chem. Biol.* **23,** 1157–1169
6. Lee, Y., Min, C. K., Kim, T. G., Song, H. K., Lim, Y., Kim, D., Shin, K., Kang, M., Kang, J. Y., Youn, H. S., Lee, J. G., An, J. Y., Park, K. R., Lim, J. J., Kim, J. H., *et al.* (2015) Structure and function of the N-terminal domain of the human mitochondrial calcium uniporter. *EMBO Rep.* **16,** 1318–1333
7. De Stefani, D., Rizzuto, R., and Pozzan, T. (2016) Enjoy the trip: calcium in mitochondria back and forth. *Annu. Rev. Biochem.* **85,** 161–192
8. De Marchi, U., Santo-Domingo, J., Castelbou, C., Sekler, I., Wiederkehr, A., and Demaurex, N. (2014) NCLX protein, but not LETM1, mediates mitochondrial Ca^{2+} extrusion, thereby limiting Ca^{2+}-induced NAD(P)H production and modulating matrix redox state. *J. Biol. Chem.* **289,** 20377–20385
9. Nowikovsky, K., Pozzan, T., Rizzuto, R., Scorrano, L., and Bernardi, P. (2012) Perspectives on: SGP symposium on mitochondrial physiology and medicine: the pathophysiology of LETM1. *J. Gen. Physiol.* **139,** 445–454
10. Pendin, D., Greotti, E., and Pozzan, T. (2014) The elusive importance of being a mitochondrial Ca^{2+} uniporter. *Cell Calcium* **55,** 139–145
11. Quan, X., Nguyen, T. T., Choi, S. K., Xu, S., Das, R., Cha, S. K., Kim, N., Han, J., Wiederkehr, A., Wollheim, C. B., and Park, K. S. (2015) Essential role of mitochondrial Ca^{2+} uniporter in the generation of mitochondrial pH gradient and metabolism-secretion coupling in insulin-releasing cells. *J. Biol. Chem.* **290,** 4086–4096
12. Sancak, Y., Markhard, A. L., Kitami, T., Kovács-Bogdan, E., Kamer, K. J., Udeshi, N. D., Carr, S. A., Chaudhuri, D., Clapham, D. E., Li, A. A., Calvo, S. E., Goldberger, O., and Mootha, V. K. (2013) EMRE is an essential component of the mitochondrial calcium uniporter complex. *Science* **342,** 1379–1382
13. Tsai, M. F., Phillips, C. B., Ranaghan, M., Tsai, C. W., Wu, Y., Willliams, C., and Miller, C. (2016) Dual functions of a small regulatory subunit in the mitochondrial calcium uniporter complex. *Elife* 10.7554/eLife.15545
14. Vais, H., Mallilankaraman, K., Mak, D. O., Hoff, H., Payne, R., Tanis, J. E., and Foskett, J. K. (2016) EMRE is a matrix Ca^{2+} sensor that governs gatekeeping of the mitochondrial Ca^{2+} uniporter. *Cell Rep.* **14,** 403–410

15. Csordás, G., Golenár, T., Seifert, E. L., Kamer, K. J., Sancak, Y., Perocchi, F., Moffat, C., Weaver, D., de la Fuente Perez, S., Bogorad, R., Koteliansky, V., Adijanto, J., Mootha, V. K., and Hajnóczky, G. (2013) MICU1 controls both the threshold and cooperative activation of the mitochondrial Ca^{2+} uniporter. *Cell Metab.* **17,** 976–987
16. Plovanich, M., Bogorad, R. L., Sancak, Y., Kamer, K. J., Strittmatter, L., Li, A. A., Girgis, H. S., Kuchimanchi, S., De Groot, J., Speciner, L., Taneja, N., Oshea, J., Koteliansky, V., and Mootha, V. K. (2013) MICU2, a paralog of MICU1, resides within the mitochondrial uniporter complex to regulate calcium handling. *PLoS One* **8,** e55785
17. Perocchi, F., Gohil, V. M., Girgis, H. S., Bao, X. R., McCombs, J. E., Palmer, A. E., and Mootha, V. K. (2010) MICU1 encodes a mitochondrial EF hand protein required for Ca^{2+} uptake. *Nature* **467,** 291–296
18. Mallilankaraman, K., Cárdenas, C., Doonan, P. J., Chandramoorthy, H. C., Irrinki, K. M., Golenár, T., Csordás, G., Madireddi, P., Yang, J., Müller, M., Miller, R., Kolesar, J. E., Molgó, J., Kaufman, B., Hajnóczky, G., *et al.* (2012) MCUR1 is an essential component of mitochondrial Ca^{2+} uptake that regulates cellular metabolism. *Nat. Cell Biol.* **14,** 1336–1343
19. Chaudhuri, D., Artiga, D. J., Abiria, S. A., and Clapham, D. E. (2016) Mitochondrial calcium uniporter regulator 1 (MCUR1) regulates the calcium threshold for the mitochondrial permeability transition. *Proc. Natl. Acad. Sci. U.S.A.* **113,** E1872–E1880
20. Pan, X., Liu, J., Nguyen, T., Liu, C., Sun, J., Teng, Y., Fergusson, M. M., Rovira, I. I., Allen, M., Springer, D. A., Aponte, A. M., Gucek, M., Balaban, R. S., Murphy, E., and Finkel, T. (2013) The physiological role of mitochondrial calcium revealed by mice lacking the mitochondrial calcium uniporter. *Nat. Cell Biol.* **15,** 1464–1472
21. Wu, Y., Rasmussen, T. P., Koval, O. M., Joiner, M. L., Hall, D. D., Chen, B., Luczak, E. D., Wang, Q., Rokita, A. G., Wehrens, X. H., Song, L. S., and Anderson, M. E. (2015) The mitochondrial uniporter controls fight or flight heart rate increases. *Nat. Commun.* **6,** 6081
22. Xu, S., and Chisholm, A. D. (2014) *C. elegans* epidermal wounding induces a mitochondrial ROS burst that promotes wound repair. *Dev. Cell* **31,** 48–60
23. Mammucari, C., Gherardi, G., Zamparo, I., Raffaello, A., Boncompagni, S., Chemello, F., Cagnin, S., Braga, A., Zanin, S., Pallafacchina, G., Zentilin, L., Sandri, M., De Stefani, D., Protasi, F., Lanfranchi, G., and Rizzuto, R. (2015) The mitochondrial calcium uniporter controls skeletal muscle trophism *in vivo*. *Cell Rep.* **10,** 1269–1279
24. Tarasov, A. I., Semplici, F., Ravier, M. A., Bellomo, E. A., Pullen, T. J., Gilon, P., Sekler, I., Rizzuto, R., and Rutter, G. A. (2012) The mitochondrial Ca^{2+} uniporter MCU is essential for glucose-induced ATP increases in pancreatic β-cells. *PLoS One* **7,** e39722
25. Gouriou, Y., Bijlenga, P., and Demaurex, N. (2013) Mitochondrial Ca^{2+} uptake from plasma membrane Cav3.2 protein channels contributes to ischemic toxicity in PC12 cells. *J. Biol. Chem.* **288,** 12459–12468
26. Qiu, J., Tan, Y. W., Hagenston, A. M., Martel, M. A., Kneisel, N., Skehel, P. A., Wyllie, D. J., Bading, H., and Hardingham, G. E. (2013) Mitochondrial calcium uniporter Mcu controls excitotoxicity and is transcriptionally repressed by neuroprotective nuclear calcium signals. *Nat. Commun.* **4,** 2034
27. Rasmussen, T. P., Wu, Y., Joiner, M. L., Koval, O. M., Wilson, N. R., Luczak, E. D., Wang, Q., Chen, B., Gao, Z., Zhu, Z., Wagner, B. A., Soto, J., McCormick, M. L., Kutschke, W., Weiss, R. M., *et al.* (2015) Inhibition of MCU forces extramitochondrial adaptations governing physiological and pathological stress responses in heart. *Proc. Natl. Acad. Sci. U.S.A.* **112,** 9129–9134
28. Rizzuto, R., De Stefani, D., Raffaello, A., and Mammucari, C. (2012) Mitochondria as sensors and regulators of calcium signalling. *Nat. Rev. Mol. Cell Biol.* **13,** 566–578
29. Csordás, G., Renken, C., Várnai, P., Walter, L., Weaver, D., Buttle, K. F., Balla, T., Mannella, C. A., and Hajnóczky, G. (2006) Structural and functional features and significance of the physical linkage between ER and mitochondria. *J. Cell Biol.* **174,** 915–921
30. Tubbs, E., Theurey, P., Vial, G., Bendridi, N., Bravard, A., Chauvin, M. A., Ji-Cao, J., Zoulim, F., Bartosch, B., Ovize, M., Vidal, H., and Rieusset, J. (2014) Mitochondria-associated endoplasmic reticulum membrane (MAM) integrity is required for insulin signaling and is implicated in hepatic insulin resistance. *Diabetes* **63,** 3279–3294
31. Szabadkai, G., Bianchi, K., Várnai, P., De Stefani, D., Wieckowski, M. R., Cavagna, D., Nagy, A. I., Balla, T., and Rizzuto, R. (2006) Chaperone-mediated coupling of endoplasmic reticulum and mitochondrial Ca^{2+} channels. *J. Cell Biol.* **175,** 901–911
32. Arruda, A. P., and Hotamisligil, G. S. (2015) Calcium homeostasis and organelle function in the pathogenesis of obesity and diabetes. *Cell Metab.* **22,** 381–397
33. Li, G., Mongillo, M., Chin, K. T., Harding, H., Ron, D., Marks, A. R., and Tabas, I. (2009) Role of ERO1-α-mediated stimulation of inositol 1,4,5-triphosphate receptor activity in endoplasmic reticulum stress-induced apoptosis. *J. Cell Biol.* **186,** 783–792
34. Bánsághi, S., Golenár, T., Madesh, M., Csordás, G., RamachandraRao, S., Sharma, K., Yule, D. I., Joseph, S. K., and Hajnóczky, G. (2014) Isoform- and species-specific control of inositol 1,4,5-trisphosphate (IP3) receptors by reactive oxygen species. *J. Biol. Chem.* **289,** 8170–8181
35. Lin, M. T., and Beal, M. F. (2006) Mitochondrial dysfunction and oxidative stress in neurodegenerative diseases. *Nature* **443,** 787–795
36. Lye, C. M., Naylor, H. W., and Sanson, B. (2014) Subcellular localisations of the CPTI collection of YFP-tagged proteins in *Drosophila* embryos. *Development* **141,** 4006–4017
37. Drago, I., and Davis, R. L. (2016) Inhibiting the mitochondrial calcium uniporter during development impairs memory in adult *Drosophila*. *Cell Rep.* **16,** 2763–2776
38. Nagai, T., Sawano, A., Park, E. S., and Miyawaki, A. (2001) Circularly permuted green fluorescent proteins engineered to sense Ca^{2+}. *Proc. Natl. Acad. Sci. U.S.A.* **98,** 3197–3202
39. Patron, M., Checchetto, V., Raffaello, A., Teardo, E., Vecellio Reane, D., Mantoan, M., Granatiero, V., Szabò, I., De Stefani, D., and Rizzuto, R. (2014) MICU1 and MICU2 finely tune the mitochondrial Ca^{2+} uniporter by exerting opposite effects on MCU activity. *Mol. Cell* **53,** 726–737
40. Raffaello, A., De Stefani, D., Sabbadin, D., Teardo, E., Merli, G., Picard, A., Checchetto, V., Moro, S., Szabò, I., and Rizzuto, R. (2013) The mitochondrial calcium uniporter is a multimer that can include a dominant-negative pore-forming subunit. *EMBO J.* **32,** 2362–2376
41. Tanaka-Matakatsu, M., Xu, J., Cheng, L., and Du, W. (2009) Regulation of apoptosis of rbf mutant cells during *Drosophila* development. *Dev. Biol.* **326,** 347–356
42. Murphy, E., Pan, X., Nguyen, T., Liu, J., Holmström, K. M., and Finkel, T. (2014) Unresolved questions from the analysis of mice lacking MCU expression. *Biochem. Biophys. Res. Commun.* **449,** 384–385
43. Kovács-Bogdán, E., Sancak, Y., Kamer, K. J., Plovanich, M., Jambhekar, A., Huber, R. J., Myre, M. A., Blower, M. D., and Mootha, V. K. (2014) Reconstitution of the mitochondrial calcium uniporter in yeast. *Proc. Natl. Acad. Sci. U.S.A.* **111,** 8985–8990
44. Jhun, B. S., Mishra, J., Monaco, S., Fu, D., Jiang, W., Sheu, S. S., and O-Uchi, J. (2016) The mitochondrial Ca^{2+} uniporter: regulation by auxiliary subunits and signal transduction pathways. *Am. J. Physiol. Cell Physiol.* **311,** C67–C80
45. Liao, Y., Hao, Y., Chen, H., He, Q., Yuan, Z., and Cheng, J. (2015) Mitochondrial calcium uniporter protein MCU is involved in oxidative stress-induced cell death. *Protein Cell* **6,** 434–442
46. Giorgi, C., Agnoletto, C., Bononi, A., Bonora, M., De Marchi, E., Marchi, S., Missiroli, S., Patergnani, S., Poletti, F., Rimessi, A., Suski, J. M., Wieckowski, M. R., and Pinton, P. (2012) Mitochondrial calcium homeostasis as potential target for mitochondrial medicine. *Mitochondrion* **12,** 77–85
47. Doan, T. N., Gentry, D. L., Taylor, A. A., and Elliott, S. J. (1994) Hydrogen peroxide activates agonist-sensitive Ca^{2+}-flux pathways in canine venous endothelial cells. *Biochem. J.* **297**, 209–215
48. Renard, D. C., Seitz, M. B., and Thomas, A. P. (1992) Oxidized glutathione causes sensitization of calcium release to inositol 1,4,5-trisphosphate in permeabilized hepatocytes. *Biochem. J.* **284**, 507–512
49. Roveri, A., Coassin, M., Maiorino, M., Zamburlini, A., van Amsterdam, F. T., Ratti, E., and Ursini, F. (1992) Effect of hydrogen peroxide on calcium homeostasis in smooth muscle cells. *Arch. Biochem. Biophys.* **297,** 265–270

50. Xu, S., Nam, S. M., Kim, J. H., Das, R., Choi, S. K., Nguyen, T. T., Quan, X., Choi, S. J., Chung, C. H., Lee, E. Y., Lee, I. K., Wiederkehr, A., Wollheim, C. B., Cha, S. K., and Park, K. S. (2015) Palmitate induces ER calcium depletion and apoptosis in mouse podocytes subsequent to mitochondrial oxidative stress. *Cell Death Dis.* **6,** e1976
51. Terentyev, D., Györke, I., Belevych, A. E., Terentyeva, R., Sridhar, A., Nishijima, Y., de Blanco, E. C., Khanna, S., Sen, C. K., Cardounel, A. J., Carnes, C. A., and Györke, S. (2008) Redox modification of ryanodine receptors contributes to sarcoplasmic reticulum Ca^{2+} leak in chronic heart failure. *Circ. Res.* **103,** 1466–1472
52. Raghu, P., and Hasan, G. (1995) The inositol 1,4,5-triphosphate receptor expression in *Drosophila* suggests a role for IP3 signalling in muscle development and adult chemosensory functions. *Dev. Biol.* **171,** 564–577
53. Dong, Z., Shanmughapriya, S., Tomar, D., Siddiqui, N., Lynch, S., Nemani, N., Breves, S. L., Zhang, X., Tripathi, A., Palaniappan, P., Riitano, M. F., Worth, A. M., Seelam, A., Carvalho, E., Subbiah, R., *et al.* (2017) Mitochondrial Ca^{2+} uniporter is a mitochondrial luminal redox sensor that augments MCU channel activity. *Mol. Cell* **65,** 1014–1028 e1017
54. Park, J., Kim, Y., Choi, S., Koh, H., Lee, S. H., Kim, J. M., and Chung, J. (2010) *Drosophila* Porin/VDAC affects mitochondrial morphology. *PLoS One* **5,** e13151
55. Min, S., Chae, H. S., Jang, Y. H., Choi, S., Lee, S., Jeong, Y. T., Jones, W. D., Moon, S. J., Kim, Y. J., and Chung, J. (2016) Identification of a peptidergic pathway critical to satiety responses in *Drosophila*. *Curr. Biol.* **26,** 814–820
56. Tennessen, J. M., Barry, W. E., Cox, J., and Thummel, C. S. (2014) Methods for studying metabolism in *Drosophila*. *Methods* **68,** 105–115
57. Kim, W., Kim, H. D., Jung, Y., Kim, J., and Chung, J. (2015) *Drosophila* low temperature viability protein 1 (LTV1) is required for ribosome biogenesis and cell growth downstream of *Drosophila* Myc (dMyc). *J. Biol. Chem.* **290,** 13591–13604
58. Budnik, V., Gorczyca, M., and Prokop, A. (2006) Selected methods for the anatomical study of *Drosophila* embryonic and larval neuromuscular junctions. *Int. Rev. Neurobiol.* **75,** 323–365
59. Tian, L., Hires, S. A., Mao, T., Huber, D., Chiappe, M. E., Chalasani, S. H., Petreanu, L., Akerboom, J., McKinney, S. A., Schreiter, E. R., Bargmann, C. I., Jayaraman, V., Svoboda, K., and Looger, L. L. (2009) Imaging neural activity in worms, flies and mice with improved GCaMP calcium indicators. *Nat. Methods* **6,** 875–881
60. Park, K. S., Wiederkehr, A., Kirkpatrick, C., Mattenberger, Y., Martinou, J. C., Marchetti, P., Demaurex, N., and Wollheim, C. B. (2008) Selective actions of mitochondrial fission/fusion genes on metabolism-secretion coupling in insulin-releasing cells. *J. Biol. Chem.* **283,** 33347–33356